Functional Materials 18, No.4 (2011)

Structure and ionic conductivity of the PEO-containing triblock copolymers forming intramolecular polycomplexes

S.V.Fedorchuk, T.B.Zheltonozhskaya, E.M.Shembel[*], L.R.Kunitskaya, I.M.Maksuta*[*], Y.P.Gomza*[**]

Department of Macromolecular Chemistry, Faculty of Chemistry, Kyiv National T. Shevchenko University, 64 Vladimirskaya St., 01033 Kyiv, Ukraine
[*]Laboratory of Electrochemical Current Sources, Ukrainian State Chemical-Engineering University, 8 Gagarin St., 49005 Dnipropetrovsk, Ukraine
[**]Institute for Macromolecular Chemistry, National Academy of Sciences of Ukraine, 48 Kharkovskoye Shosse, 02160 Kyiv, Ukraine

Received July 7, 2011

A series of structural and electrochemical studies of the triblock copolymers (TBC) based on poly(ethylene oxide) (M_v = 3, 15, 35, 40 and 100 kDa) and polyacrylamide (PAAm-*b*-PEO-*b*-PAAm), which formed the intramolecular polycomplexes, were carried out using NMR, WAXS, SAXS and impedance spectroscopy. The combination of the amorphous mass-fractal-organized structure of the copolymers (in the region of M_{vPEO} up to ~40 kDa) with high level of the ionic conductivity of pure TBCs and their compositions with $LiPF_6$ was established. Possible reasons for the effects in the context of using of TBC compositions in lithium batteries are discussed.

Проведена серия структурных и электрохимических исследований триблок-сополимеров (ТБС), основанных на полиэтиленоксиде (M_v = 3, 15, 35, 40 и 100 кДа) и полиакриламиде (ПАА-*b*-ПЕО-*b*-ПАА), которые образовывали интрамолекулярные поликомплексы, с использованием ЯМР, WAXS, SAXS и импедансной спектроскопии. Установлено сочетание аморфной массово-фрактально-организованной структуры сополимеров (в области $M_{vПЕО}$ до ~40 кДа) с высоким уровнем ионной проводимости чистых ТБС и их композиций с $LiPF_6$. Обсуждены возможные причины таких эффектов в контексте использования композиций ТБС в литиевых батареях.

1. Introduction

The structure of polymer materials is the main factor defining their physical and functional characteristics. This explains the great interest in studies of different structural problems and the appearance of numerous original works and monographs in this area [1–3]. Most of the studies in the field of block copolymers are devoted to those containing thermodynamically immiscible or limitedly miscible polymer components [1–5]. However, the block copolymers with chemically complementary components, which are capable of forming the system of cooperative non-covalent bonds such as electrostatic or hydrogen bonds, are of special interest. These block copolymers belong to the class of intramolecular polycomplexes (IntraPC) [6]. The block structure of IntraPCs in dependence on the total and relative length of polymer components and their character (amorphous or crystalline) has not been sufficiently well studied.

In recent years significant attention has been paid to PEO-containing diblock and triblock copolymers [7], which have many potential applications as ion-conducting ma-

trices in different electrochemical devices, in particular, in solid-state lithium batteries [8]. Due to the presence of crystallizable PEO chains in the structure of block copolymers alongside with amorphous components such as poly(propylene oxide), polystyrene, poly[alkyl(meth)acrylates], it can be possible to reduce sharply the undesirable crystallization of PEO, thus maintaining high mobility of its segments and ensuring a high level of the block copolymer conductivity [7]. The largest decrease in the crystallinity degree was observed in the triblock copolymers with PEO central block and two side amorphous blocks [1, 9]. When the length of side blocks became larger than a certain critical value, which depended on their chemical nature and PEO length, the triblock copolymers completely lost their capability of crystallization [1]. An additional decrease in PEO crystallinity and increase in the conductivity could be expected in the PEO-containing block copolymers forming IntraPCs, though ionic conductivity of such copolymers was not studied.

Polyacrylamide (PAAm) and poly(ethylene oxide) (PEO) are a couple of chemically complementary polymers that form a hydrogen-bonded intermolecular polycomplex (InterPC) at their mixing in aqueous medium [10]. The existence of H-bond system between PEO and PAAm chains was proved also in the PAAm-*b*-PEO-*b*-PAAm triblock copolymers (TBCs) [11]. Also, an important effect of a stronger interaction of covalently bound PEO and PAAm chains in TBCs as compared to the polymer mixtures with the same content has also been established. It was shown [12] that due to existence of long amorphous chains of PAAm and the IntraPC formation, the TBC structure preserved its amorphous character also at a large length of the PEO central block (up to M_v ~ 40 kDa). Thermodynamic compatibility of PEO and PAAm blocks essentially improved after transition of TBC samples through the melting point; resulting in the copolymer structure becoming still more homogeneous [12]. These facts, as well as the known ability of PEO oxygen atoms [7, 8] and PAAm amide groups [13] to attach Li+ ions, were the main reason to proceed with detailed investigations of TBC bulk structure and to study the ionic conductivity of their compositions with lithium salt ($LiPF_6$).

2. Experimental procedure

Syntheses. In TBC syntheses we used poly(ethylene glycol) with M_v = 3 (PEG1), 15 (PEG2), 40 (PEG3), 100 (PEG4) and 35 kDa (PEG5) obtained from Aldrich, USA, cerium ammonium nitrate (initiator) from the same source, as well as acrylamide (AA) re-crystallized from chloroform (Merck, Germany). The syntheses were carried out in deionized water by the radical block copolymerization with participation of PEO radicals, which were formed due to redox reaction between terminal hydroxyl groups and cerium (IV) ions [6, 11]. The samples of TBC1–TBC5 (according to the number of initial PEG) were obtained at the constant molar ratios of the reagents: $[Ce^{IV}]/[PEG] = 2$ and $[Ce^{IV}]/[AA] = 1 \cdot 10^{-3}$. At the same time, the total concentration of all the reagents was increased by 1.53 times in the case of TBC2, TBC3 and TBC5. The reaction blend was mixed in an inert atmosphere at 20°C for 24 h. Homopolymerization of AA was carried out in similar conditions using ethanol instead of PEG ($[Ce^{IV}]/[C_2H_5OH] = 1$). The (co)polymer samples were re-precipitated by acetone, dissolved in water and freeze dried.

The molecular structure characterization. In order to confirm the chemical structure of TBCs and to determine the molecular weights of PAAm blocks and TBC macromolecules, the nuclear magnetic resonance (NMR) spectroscopy was applied. ^1H NMR spectra in deuterated water (C = 10 kg·m^{-3}) were recorded at 400 MHz and 20°C using a Mercury-400 instrument from "Varian" (USA). The chemical shifts (δ) were determined with respect to tetramethylsilane as a reference. The relative integral intensities of the proton signals were calculated from the spectra using NUTS program. Molecular parameters of two TBC samples were determined also by an elemental analysis. The molecular weight of PAAm was found by viscometry (M_v = 630 kDa).

Wide-angle X-ray scattering. The bulk structure of TBCs was characterized first by WAXS. The scattering profiles for TBCs, PAAm and PEGs were obtained using a DRON-2.0 X-ray diffractometer. The copolymer films were cast from aqueous solutions onto Teflon surface and dried in a vacuum case for one week. The film piles with thickness of ~1 mm were used for these measurements. The monochromatic $Cu–K_\alpha$ radiation with λ = 0.154 nm, filtered by Ni, was provided by an IRIS-M7 generator at the operating voltage of 30 kV and current of 30 mA. The scattering intensities were measured by a scintillation detector scanning in 0.2° steps over the range of the

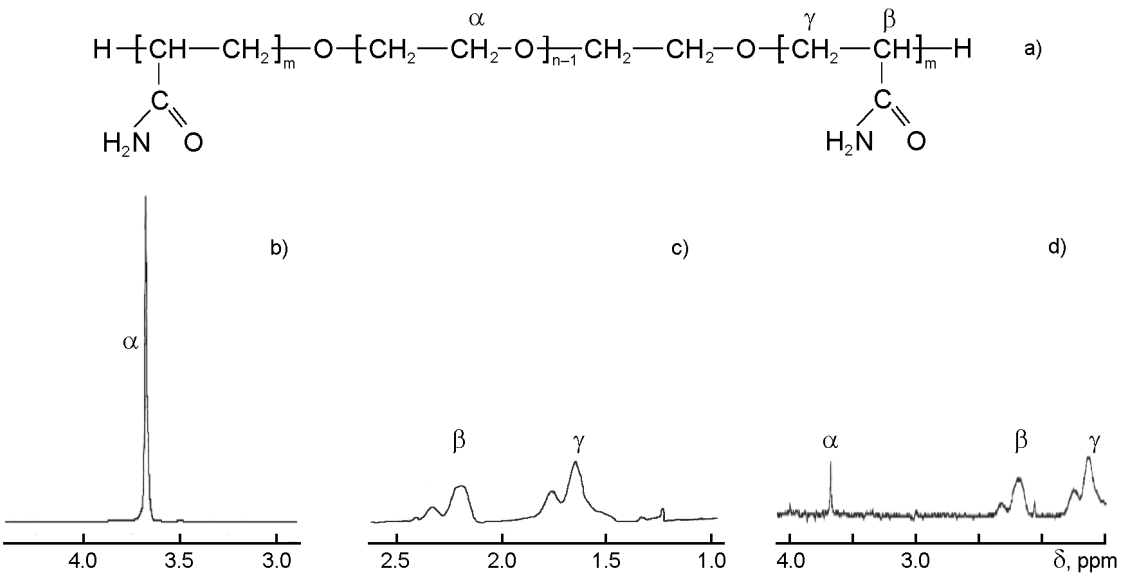

Fig. 1(a) Chemical formula of TBCs and examples of ^{1}H NMR spectra for: (b) PEG3, (c) PAAm and (d) TBC3 in D_2O. T = 20°C.

θ = 3–40° scattering angles. The diffraction curves obtained were reduced to equal intensities of the primary beam and equal values of the scattering volume [14]. Also, the normalization of experimental scattering intensities was carried out according to the formula:

$$I_{n(i)}(\theta) = [I_{\exp}(\theta) - I_b(\theta)] \cdot (I/I_0), \qquad (1)$$

were $I_{exp}(\theta)$ and $I_{n(i)}(\theta)$ are the experimental and normalized intensities in WAXS profile as a function of θ, $I_b(\theta)$ is the intensity of the background for every θ value, I_0 and I are the intensities of incident and scattered beams at θ = 0° (the beam attenuation coefficient). Moreover, the additive scattering curves were calculated for PEG+PAAm mixtures, compositions of which corresponded to those in respective TBCs, using the relationship:

$$I_{n(PAAm+PEG)}(\theta) = \qquad (2)$$
$$= I_{n(PAAm)}(\theta) \cdot w_{PAAm} + I_{n(PEO)}(\theta) \cdot w_{PEO},$$

where w_{PAAm} and w_{PEO} are the weight fractions of PEO and PAAm in the copolymers.

Small-angle X-ray scattering. SAXS experiments were carried out using an automated Kratky slit-collimated camera. Here we used copper anode emission, which was monochromated by a total internal reflection and nickel filter. The intensity curves were recorded in the step-scanning mode of the scintillation detector in the θ = 0.03–4.0° region, which corresponded to the wavevector region q = 0.022–2.86 nm^{-1} [where $q = 4\pi \cdot \sin(\theta/2)/\lambda$]. Thus, the microscale heterogeneous domains with dimensions (evaluated as $2\pi/q$) from 2 to 280 nm could be characterized. Preliminary processing of SAXS profiles was carried out using the FFSAXS-3 program [15]. To reduce the SAXS data to the absolute scale a standard reference sample from the laboratory of professor Kratky was used. The scattering intensity of a (co)polymer was normalized to the sample thickness and the scattering intensity of an etalon. In order to calculate the microphase structure parameters the raw intensity curves were smoothed, corrected for parasitic scattering and desmeared.

The ionic conductivity measurements. The films (~5×5 cm^2) of pure TBC5 and its mixtures with lithium perfluoro phosphate were cast from aqueous solutions onto Teflon surface and dried on air for 3–4 days and then in a vacuum-case. The specific ionic conductivity was determined by impedance spectroscopy [16]. All the experiments were carried out in a special cell with Pt electrodes in the frequency region 0.001–100 kHz at T = 20°C using a Voltalab (USA) instrument with a computer program Voltalab Master. According to the measuring protocol, dry films were squeezed between the electrodes in a cell. In some cases a plasticizer ethylene glycol (EG) was additionally introduced in the compositions.

Table 1. Molecular parameters of the triblock copolymers found by (1) elemental analysis and (2) NMR spectroscopy

Copolymer	Method	M_{vPEO}, kDa	M_{PAAm}, kDa	M_{TBC}, kDa	w_{PEO} [a], %	n [b]
TBC1	1	3	45	94	3.2	9.4
	2		67	37	2.2	10.8
TBC2	2	15	230	475	3.2	9.5
TBC3	2	40	833	1706	2.3	12.9
TBC4	1	100	907	1914	5.2	5.6
TBC5	2	35	1823	3681	1.0	32.3

[a] The weight part of PEO in the copolymers.

[b] The ratio between units of PAAm and PEO blocks in the copolymers, base-mole$_{PAAm}$/base-mole$_{PEO}$

3. Results and discussion

Examples of ^{1}H NMR spectra are shown in Fig. 1. The proton signal of methylene groups (α) with δ = 3.68 ppm was displayed in the spectra of PEG (Fig. 1a). The proton signals of methine (β) and methylene (γ) groups with δ = 1.4–1.8 and 2.1–2.4 ppm, respectively, were observed in the spectrum of PAAm (Fig. 1b). The spectra of the copolymer samples contained all the signals pointed (Fig. 1c), thus confirming the presence of PEO and PAAm blocks in TBC macromolecules. Using the integral intensities (A) of the signals α and β or α and γ as well as the known molecular weights of PEGs, the molecular weights of PAAm side blocks were calculated according to:

$$M_{n\cdot PAAm} = \frac{2 \cdot M_{0\cdot PAAm} \cdot M_{PEO} \cdot A_b}{M_{0\cdot PEO} \cdot A_a}$$

or

$$M_{n\cdot PAAm} = \frac{M_{0\cdot PAAm} \cdot M_{PEO} \cdot A_c}{M_{0\cdot PEO} \cdot A_a}. \qquad (3)$$

Here $M_{0\ PAAm}$ and $M_{0\ PEO}$ are the molecular weights of PEO and PAAm units. Such calculations for block copolymers are widely used in modern literature [17]. The molecular weights of TBCs were calculated by equation:

$$M_{TBC} = 2 \cdot M_{PAAm} + M_{PEO}. \qquad (4)$$

Molecular parameters of TBCs found by elemental analysis and ^{1}H NMR are shown in Table 1. It can be seen that TBC1–TBC4 samples constitute a series of the copolymers with increasing length of PEO and PAAm blocks.

The results of structural studies of PEG, PAAm and TBCs by WAXS are presented in Fig. 2. WAXS profile of PAAm (Fig. 2a) contained two diffusive overlapped maximums in full accordance with [18]. This effect could be attributed to the presence of two systems of planes of a paracrystalline lattice in the PAAm amorphous structure [14].

Table 2. The diffraction maximum positions in WAXS profiles and corresponding interplane distances

Polymer	The maximum positions		The average interplane distances	
	θ_1, degrees	θ_2, degrees	d_1, nm	d_2, nm
PAAm	15	22.10	~0.590	0.402
TBC1		21.60		0.411
TBC2		22.26		0.399
TBC3	15	22.56	~0.590	0.394
TBC4		21.74		0.408
TBC5		21.60		0.411

The first maximum (θ ~ 15°) with smaller intensity characterized the lateral periodicity in the arrangement of PAAm chains [14]. The second one (θ = 22.1°) with greater intensity was caused (according to the data of FTIR spectroscopy [11]) by a periodic arrangement of the flat hydrogen-bonded *cis*-dimmers of amide groups in the structures of *cis-trans*-multimers. The average interplane distances in the PAAm paracrystalline lattice were found using (5) [14]:

$$d = \frac{\lambda}{2 \cdot \sin(\theta/2)}, \qquad (5)$$

where λ is the wavelength of X-ray radiation. They are presented in Table 2. WAXS profiles of PEGs (one example is shown in

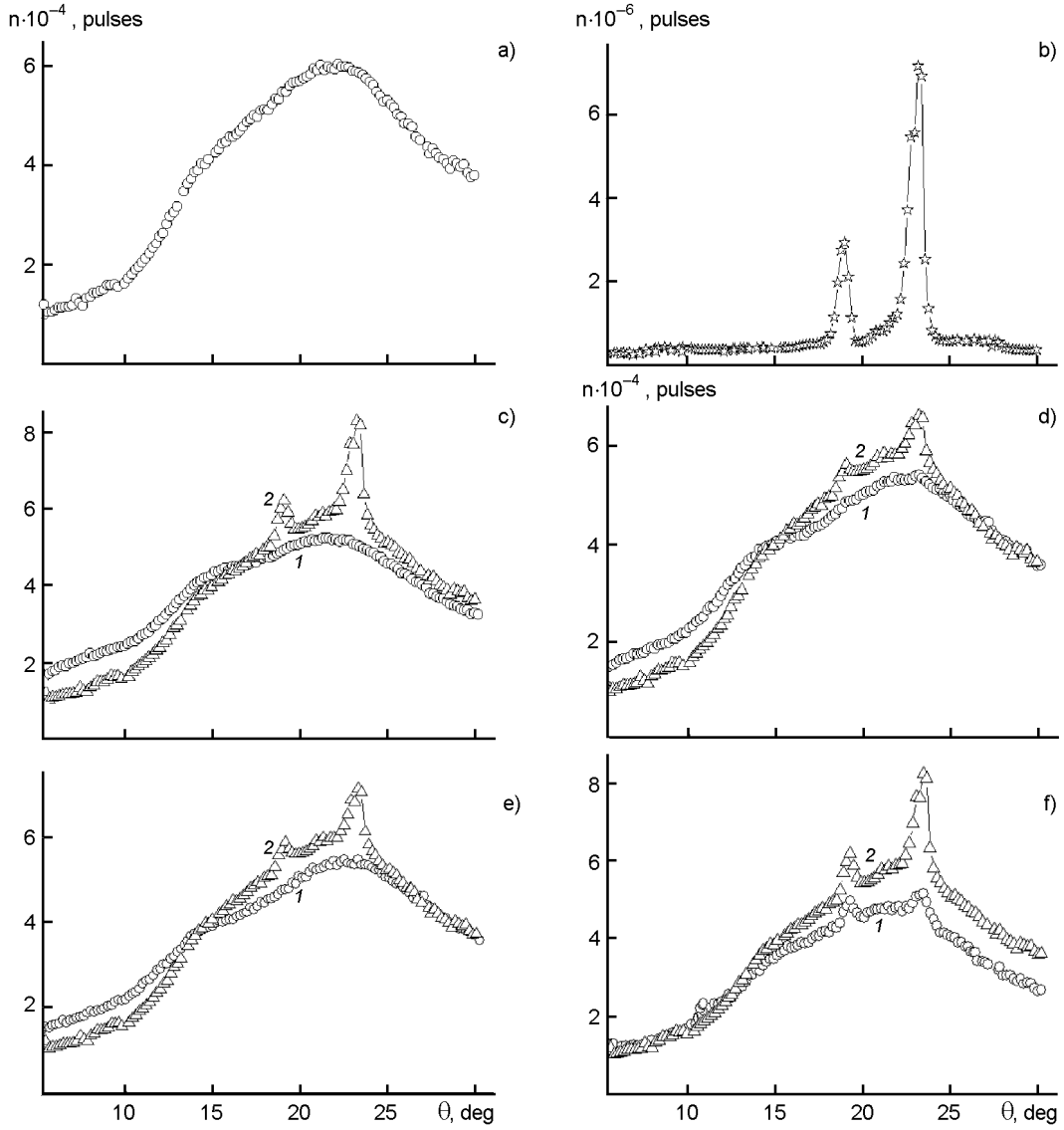

Fig. 2. WAXS profiles (the scattering intensities vs the scattering angle) for: (a) PAAm, (b) PEG1, (c) TBC1, (d) TBC2, (e) TBC3, and (f) TBC4. Experimental data and additive curves calculated for corresponding (PAAm + PEG) blends are shown. T = 25°C. For TBC5 analogous data as for TBC2 were obtained.

Fig. 2b) demonstrated two intense crystalline peaks at θ = 19.0° and 23.1°, which are well known from the literature [14].

WAXS profiles of the copolymers, except TBC4 (Fig. 2c–e, curves *1*), did not contain any crystalline peaks in spite of appearance of such peaks in the corresponding additive curves (curves *2*). The latter were calculated from (2) for PAAm+PEG blends with the same composition as in corresponding TBC samples using the assumption about independent contributions of the both components to the total scattering intensity. Small crystalline peaks of PEO were observed only in the profile of TBC4 (Fig. 2f, curve *1*), which contained the longest central block. However, the peak intensities turned out to be lower than in the additive curve. Therefore, full correlation of these results with earlier DSC data [12] was obvious.

Basing on Methues approach [2, 3], it is possible to calculate the ratio between areas under all crystalline peaks and the total WAXS curve and then to find (for homopolymers) the relative crystallinity degree. However, determination of this very appropriate parameter loses any sense in the case of heteropolymers. That is why, in order to estimate the alterations in the crystallinity degree of PEO in TBC4 structure, the ratio between the crystalline peak areas in the additive curve *2* and the experimental curve

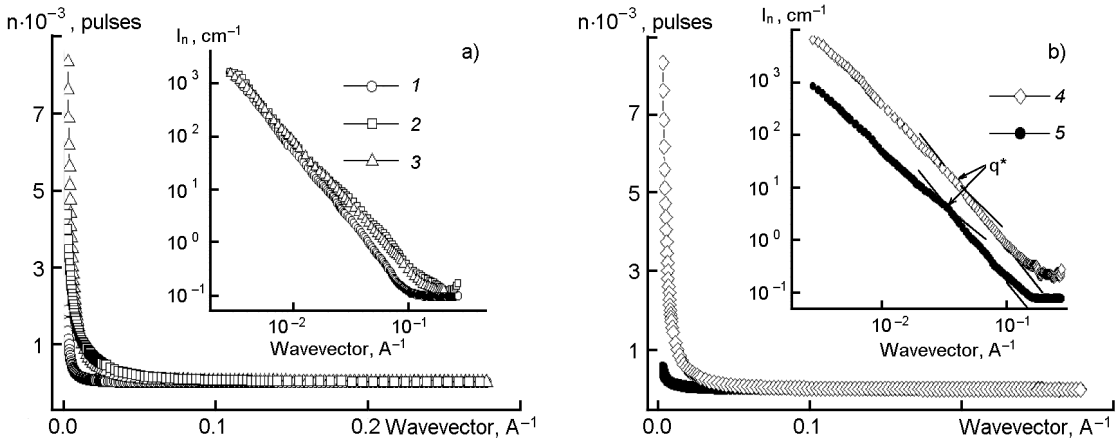

Fig. 3. The intensity of small-angle X-ray scattering vs the wavevector for: (a) PAAm — *1*, TBC1 — *2*, TBC2 — *3* and (b) TBC3 — *4*, TBC4 — *5*. Dependences of the normalized intensity vs the wavevector in the double logarithmic coordinates are shown on a smaller scale. T = 25°C. The data for TBC5 practically coincided with those for TBC2.

1 (Fig. 2f) was calculated. According to such procedure, the crystallinity degree of the initial PEG decreased by 2.9 times in TBC4 structure. This result was in full accordance with the reduction by 2.8 times in the crystallinity degree (X_c) of PEO in TBC4, which was established by DSC method in [12].

WAXS profiles of amorphous TBC1–TBC3 and TBC5 were similar to the difractogram of pure PAAm. Some differences consisted in an appreciable reduction in the relative intensity of the second maximum and alteration of its position (Fig. 2, Table 2). This effect indicates the changes in disposition of the H-bonded *cis*-dimmers of amide groups in *cis-trans*-multimers.

SAXS investigations allowed characterizing the block copolymer morphology at the supramolecular level [2, 14]. SAXS profiles of TBCs and PAAm are shown in Fig. 3.

A sharp smooth decay in the scattering intensities versus the wavevector (without any peaks or diffusive maxima) was observed for all the (co)polymer samples, thus suggesting the absence of any periodicity in the arrangement of separate structural elements of PAAm and TBCs at the supramolecular level. Then the same profiles were normalized to the thickness of (co)polymer samples and the scattering intensity of the etalon and further were represented in double logarithmic coordinates (plots in the inserts, Fig. 3) in order to carry out their detailed analysis according to the known conception about the formation of the fractal aggregates or clusters [15].

For PAAm and TBC1, TBC2, TBC5 (with relatively short PEO blocks) the linear decrease in log I_n versus log q (Fig. 3a) with the same slope was observed practically over the whole region of the wavevectors under study. This fact reflects the existence in SAXS profiles of the (co)polymers of the only Porod's power scattering regime ($I \approx q^{-Df}$) [15]. Such form of SAXS curves in the double logarithmic coordinates corresponds to the scattering picture in the system where single-level fractal clusters exist [15, 19]. The character of these clusters (mass-fractal or surface-fractal ones) could be determined by analysis of the slope ratio modulus (D_f), but the maximum diameter of the clusters could be estimated by the relation $d_{max} \sim 2\pi/q^*$ in the case when the straight line of the Porod's power scattering law transforms at small q values into the curve described by the Gineau exponential scattering law. In fact, the Gineau scattering curve "cuts" the region of the Porod power scattering. The "cutting boundary" corresponds to a definite q^* value in the range of Gineau's scattering, which is used to estimate d_{max}. Thus, the exponential Gineau scattering regime and the corresponding Porod scattering regime (at larger q values) characterize a single structural level. Unfortunately, the curves in Fig. 3a for PAAm and the given TBC samples had no "cutting borders" at small q; therefore, determination of d_{max} was impossible in these cases.

The D_f values turned out to be less than 3 for PAAm, TBC1, TBC2 and TBC5 (Table 3). It means that the amorphous structure of these (co)polymers had a porous character and consisted of mass-fractal clusters with the fractal dimension of D_f

Table 3. Parameters of separate structural elements of PAAm and TBCs found from SAXS data

Value	Polymer							
	PAAm	TBC1	TBC2	TBC3		TBC4		TBC5
$-D_f$	2.7	2.2	2.3	2.4	3.1	2.4	2.8	2.4
$q^*\cdot 10^2$ [a], A^{-1}	–	–	–	–	0.36	–	0.34	–
d_{max} [b], nm	–	–	–	–	17.2	–	18.6	–
R_g, nm	–	–	–	–	6.7	–	7.2	–

[a] "The cutting border" for the power scattering regime

[b] The maximum diameter of the mass- or surface-fractal clusters

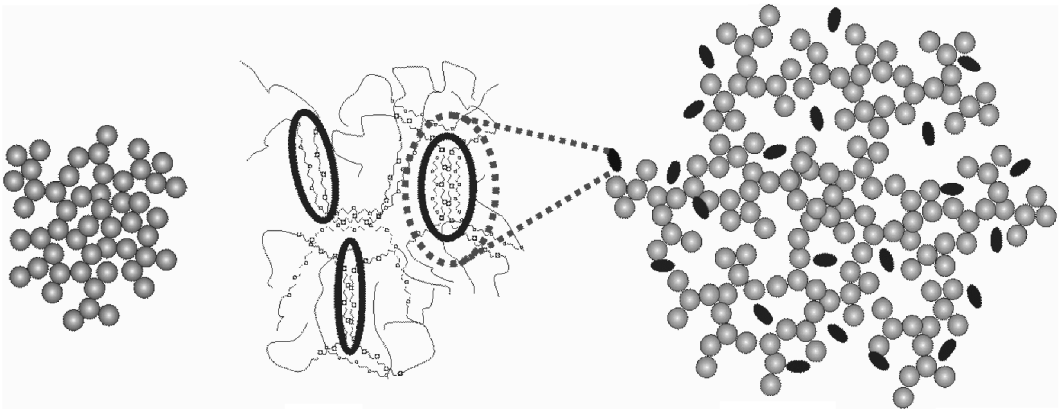

Fig. 4. The construction of (a) a single mass-fractal cluster in amorphous regions of PAAm and TBCs, (b) the surface-fractal clusters with crystalline "core" of PEO blocks, and (c) an amorphous mass-fractal-organized structure of TBC3–TBC4, where the surface-fractal clusters are distributed.

[19]. The construction of the branched mass-fractal clusters is shown in Fig. 4a.

Obviously, the fragments of the (co)polymer chains could be considered as separate "building blocks" of such clusters. At the same time, the main reason for appearance of these clusters in PAAm and TBC structure consists in high hydrophility of the (co)polymers. Indeed, the equilibrium humidity of TBC and PAAm films, which were used in SAXS experiments, is of significant value (~10 wt. %) according to the data of DTGA. This is conditioned by the capability of each amide group of PAAm and each oxygen atom of PEO to adsorb and to keep up to 4 and 2 water molecules, consequently. As a result, even the prolonged drying of the (co)polymer samples in a vacuum box and a vacuum desiccator did not provide full removing of water from them.

The double logarithmic SAXS profiles of TBC3 and TBC4 (Fig. 3b), which contained the longest PEO chains, demonstrated two linear parts with different slope ratios (two Porod's regimes) and one intermediate region corresponding to the Gineau scattering regime [15]. The values of D_f turned out to be 3.1 and 2.8 (for TBC3 and TBC4, consequently) in the 1-st Porod's regime (at higher q) and 2.4 in the 2-nd Porod's scattering regime (at less q). Such form of SAXS profiles indicates the existence of two types of fractal clusters in TBC3 and TBC4 structures, i.e., their two-level fractal organization [19]. It is evident that the effect is related to the appearance of PEO nanocrystalline domains in an amorphous matrix. Really, a sharp enough increase in the slope ratio modulus of the dependences $\log I_n = f(\log q)$ up to $D_f \approx 3$ at some intermediate q^* values (Table 3) could be interpreted as arising of the surface-fractal clusters in TBC structure. The scattering law is described in this case by the other power function: $I \approx q^{Ds-6}$ [15]. In the last formula the value $D_s = 6-D_f$ characterizes the fractal dimension of the surface-fractal clusters. Formation of the surface-fractal clusters in TBC3 and TBC4 structures occurs, evidently, due to a partial crystallization of PEO blocks belonging to several copolymer macromolecules. A scheme in Fig. 4b illustrates this process.

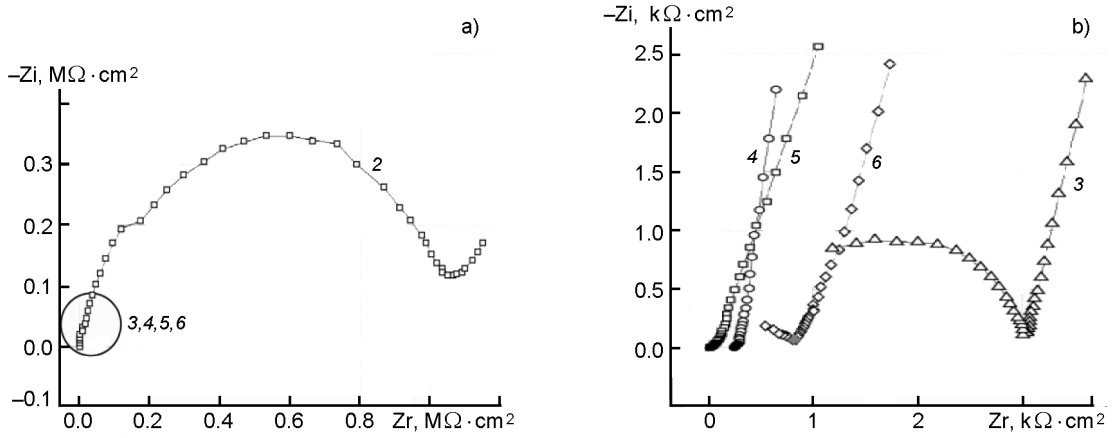

Fig. 5. The complex impedance spectra (Nyquist plots) for the following composite films: (a) TBC3+$LiPF_6$ — *2*, (b) TBC3+$LiPF_6$ — *3*, *4* and TBC3+$LiPF_6$+EG — *5*, *6* at the ratios of [TBC]/[$LiPF_6$] = 10.0 — *2*, *5*, 5.7 — *3* and 4.0 base-mol·mol^{-1} — *4*, *6*. The ratio of [EG]/[TBC] = 0.01 w/w was constant in all the three-component systems. T = 20°C. The spectrum view for a pure TBC5 was analogous to the curve *2*.

Table 4. Ionic conductivity of the triblock copolymer doped with lithium salt

Sample	System	[PEO]/[$LiPF_6$] base-mol·mol^{-1}	[TBC]/[$LiPF_6$] base-mol·mol^{-1}	l, μm	Calculating procedure	σ, S·cm^{-1}
1	TBC5	–	–	90	LE	$2.90 \cdot 10^{-6}$
2	TBC5+$LiPF_6$	0.15	10.0	100	LE	$7.52 \cdot 10^{-6}$
3	TBC5+$LiPF_6$	0.09	5.7	125	ES	$1.43 \cdot 10^{-5}$
4	TBC5+$LiPF_6$	0.06	4.0	109	LE	$1.74 \cdot 10^{-5}$
					ES	$1.93 \cdot 10^{-5}$
5	TBC5+$LiPF_6$+EG	0.15	10.0	161	LE	$8.67 \cdot 10^{-6}$
					ES	$2.22 \cdot 10^{-5}$
6	TBC5+$LiPF_6$+EG	0.06	4.0	170	LE	$1.53 \cdot 10^{-4}$

Taking into consideration that SAXS profiles of TBC3 and TBC4 contained the "cutting borders" for the 1-st scattering regime by Porod (at higher q), we have found corresponding q^* numbers in the areas of Gineau's scattering and calculated the maximum diameters ($d_{max} \sim 2\pi/q^*$) and the gyration radii [$R_g = d_{max}/2(5/3)^{1/2}$] of the surface-fractal clusters with crystalline "core" of PEO (Table 3) [15]. Thus, the conclusion about two fractal levels (they are shown in Fig. 4c) in the structures of TBC3 and TBC4 unlike to those of TBC1, TBC2 and TBC5 has been achieved. The small surface-fractal clusters with a crystalline "core" of PEO blocks formed the first level but the large mass-fractal clusters of an amorphous matrix constituted the second one.

Due to these studies, the amorphous character and homogeneity of TBC structure at different levels in a wide region of the PEO block length and also its porosity were established. The sample of TBC5 with exactly such structure was used in the following studies of the ionic conductivity. The specific ionic conductivity of a pure TBC5 and its compositions with lithium salt, where the electrolyte content was varied relatively to the copolymer, was measured by an impedance spectroscopy [16]. Frequency dependences of the imaginary and real parts of the complex impedance (Nyquist plots) are represented in Fig. 5. In order to enhance the polymer segment mobility, a nonionic plasticizer ethyleneglycol (EG) with the constant weight fraction (1 wt. % from TBC weight) was added in two cases (Table 4). Significant increase in the film elasticity took place upon introduction of $LiPF_6$ and EG.

The volume resistances of the films were determined by two procedures: (LE) the linear extrapolation of experimental data to

the abscissa-axis in the region of high frequencies and (ES) the extrapolation of the high frequency semicircles observed in some plots to the abscissa-axis [20]. The specific ionic conductivity was calculated using the (6) relation [21]:

$$\sigma = \frac{l}{R \cdot S}, \quad (6)$$

where l is the film thickness, S is the electrode area, R is the volume resistance of a film. All the results obtained are shown in the right-hand part of Table 4. It is seen that even the film of pure TBC5 demonstrated a high level of the ionic conductivity. This could be explained first by the above-mentioned high hydrophility of the copolymer components resulting in high equilibrium humidity of TBC films. Further, PEO chains lose their ability to crystallization because of interaction with PAAm that keeps their mobility and promotes a conductivity growth. Finally, the porous mass-fractal organization of TBC structure that contains the absorbed water possibly remaining in the copolymer sample after synthesis (see the above synthetic strategy), ensures free ion transport through the copolymer films under the action of electric field.

A considerable increase in the ionic conductivity of the copolymer films takes place with growth of the lithium salt content. This effect is not surprising and could be interpreted by increase in the concentration of the charge carriers and the plasticizing action of lithium salt on TBC structure (the plasticizing effect of Li^+ salts on the structure of the PEO-containing block copolymers is well-known from the literature [7]). Introduction of a small quantity of the non-ionic plasticizer EG not only improves elasticity of the composite films but also raises essentially their conductivity. According to the data of Table 4, the increase in the lithium salt content and also the plasticizer addition act in the same direction. Thus, due to application of TBC films doped by $LiPF_6$ and small additives of EG a high level of the ionic conductivity ($\sigma = 1.53 \cdot 10^{-4}$ S·cm^{-1} at 20°C) could be achieved.

It would be interesting to compare the ionic conductivity of different PEO-containing block copolymers and their composites. Unfortunately, the dependence of σ on too many factors — such as a molecular weight of PEO blocks, a chemical nature, a physical state and molecular parameters of other blocks, a molecular architecture and a structural organization of block copolymers, moreover, a chemical origin and concentration of electrolytes (and/or other additives) and also the conditions of formation and testing of the block copolymer composites — does not allow a detailed comparison of σ values in different systems. Therefore, to show the level of the ionic conductivity of TBC films, we will give only three maximum values of σ, which were reached in the systems: i) the partially crystalline multiblock copolymers $[PEO\text{-}b\text{-}PPO\text{-}b\text{-}PS]_n$, including poly(propylene oxide) and polystyrene, in composition with $LiClO_4$ ($\sigma \sim 2 \cdot 10^{-4}$ S·cm^{-1} at 25°C) [22], ii) the partially crystalline multiblock copolymer $[PEO\text{-}b\text{-}PPO]_n/LiClO_4$ ($\sigma = 5.8 \cdot 10^{-4}$ S·cm^{-1} at 25°C) [22] and iii) the multiblock copolymers with polybutadiene $[PEO\text{-}b\text{-}PB\text{-}b\text{-}PS]_n/LiClO_4$ ($\sigma \sim 1 \cdot 10^{-4}$ S·cm^{-1} at 35°C) [23].

4. Conclusions

Formation of IntraPC in TBC macromolecules prevents crystallization of PEO blocks and provides existence of a homogeneous amorphous structure in a wide region of their molecular weights. At the same time, at $M_{vPEO} \geq 40$ kDa the homogeneity of TBC structure is broken due to partial crystallization of PEO blocks. As a result, small surface-fractal clusters with nanocrystalline "core" of PEO blocks having the maximum radius of gyration $R_g \sim 7$ nm appear among the large mass-fractal clusters of an amorphous matrix. Basing on experimental results and above discussion, the following key structural factors, which ensure the high ionic conductivity of pure and doped PAAm-*b*-PEO-*b*-PAAm films, could be picked out: i) the existence of the hydrogen bond system between PEO and PAAm blocks, due to which PEO chains lose their ability to crystallize, ii) the homogeneous distribution of the regions containing hydrogen-bonded segments of both components in the copolymer structure, iii) the porous mass-fractal-organization of TBC structure, which promotes a free and quick transport of electrolytes through composite films.

References

1. V.P.Privalko, V.V.Novikov, The Science of Heterogeneous Polymers. Structure and Thermophysical Properties, John Wiley & Sons, Chichester etc. (1995).
2. I.W.Hamley, Crystallization in Block Copolymers. Advances in Polymer Science, Springer-Verlag, Berlin-Heidelberg (1999).
3. I.W.Hamley, The Physics of Block Copolymers, Oxford University Press, Oxford (1998).
4. I.W.Hamley, V.Castelletto, *Prog. Polym. Sci.*, **29**, 909 (2004).
5. N.Hadjichristidis, S.Pispas, G.Floudas, Block Copolymers. Synthetic Strategies, Physical Properties and Applications, Wiley, New York (2003).
6. T.Zheltonozhskaya, N.Permyakova, L.Momot, in: Hydrogen-Bonded Interpolymer Complexes: Formation, Structure and Applications, Ch.5, World Scientific Publ. Co., New Jersey, London, Singapore etc. (2009).
7. H.-Q.Xie, D.Xie, *Prog. Polym. Sci.*, **24**, 275 (1999).
8. F.M.Gray, Polymer Electrolytes, The Royal Society of Chemistry Monographs, Cambridge, London (1997).
9. H.-Q.Xie, P.G.Zhou, Multicomponent Polymer Materials, in: Adv. Chem. Ser., No. 211, ACS, Washington DC (1986).
10. L.Momot, T.Zheltonozhskaya, N.Permyakova et al., *Macromol. Symp.*, **222**, 209 (2005).
11. N.M.Permyakova, T.B.Zheltonozhskaya, V.V.Shilov et al., *Theor. Exper. Chem.*, **41**, 382 (2005).
12. T.B.Zheltonozhskaya, S.V.Fedorchuk, Yu.P.Gomza et al., *Questions Chem. Chem. Technol.*, No.2, 78 (2007).
13. M.H.Baron, F.Fillaux, *Can. J. Chem.*, **63**, 1473 (1985).
14. Yu.S.Lipatov, V.V.Shilov, Yu.P.Gomza et al., X-Ray Diffraction Methods to Study Polymeric Systems, Naukova Dumka, Kyiv (1982) [in Russian].
15. A.P.Shpak, V.V.Shilov, O.A.Shilova et al., Diagnostics of Nanosystems. Multilevel Fractal Structures, Naukova Dumka, Kyiv (2004) [in Russian].
16. E.Barsoukov, J.R.Macdonald, Impedance Spectroscopy. Theory, Experiment and Applications, 2-nd ed. Wiley & Sons, New York (2005).
17. F.Meng, S.Zheng, T.Liu, *Polymer*, **47**, 7590 (2006).
18. U.M.Korolev, T.G.Veretyahina, V.V.Chupov et al., *Vysokomol. Soedin. Ser. A*, **37**, 1160 (1995).
19. G.Beaucage, J.Hyeonlee, Se.Pratsinis et al., *Langmuir*, **14**, 5751 (1998).
20. P.G.Bruce, *Solid State Ionics*, **15**, 247 (1985).
21. G.B.Appetecchi, W.Henderson, P.Villano et al., *J. Electrochem. Soc.*, **148**, A1171 (2001).
22. H.-Q.Xie, Z.S.Liu, J.S.Guo, *Polymer*, **35**, 4914 (1994).
23. H.-Q.Xie, X.Q.Tao, J.S.Guo, *J. Appl. Polym. Sci.*, **61**, 407 (1996).

Структура та іонна електропровідність ПЕО-вмісних триблок-кополімерів, що формують інтрамолекулярні полікомплекси

С.В.Федорчук, Т.Б.Желтоножська, О.М.Шембель, Л.Р.Кунитська, І.М.Максюта, Ю.П.Гомза

Проведено серію структурних та електрохімічних досліджень триблок-кополімерів (ТБК), основаних на поліетиленоксиді (M_v = 3, 15, 35, 40 та 100 кДа) та поліакриламіді (ПАА-*b*-ПЕО-*b*-ПАА), які утворювали інтрамолекулярні полікомплекси, використовуючи ЯМР, WAXS, SAXS та імпедансну спектроскопію. Встановлено поєднання аморфної масово-фрактально-організованої структури кополімерів (в області $M_{vПЕО}$ до ~40 кДа) з високим рівнем йонної провідності чистих ТБК та їх композицій з $LiPF_6$. Обговорено можливі причини таких ефектів у контексті використання композицій ТБК у літієвих батареях.